Microstructure and Properties of Iron Aluminide Coatings

R.N. Wright
Idaho National Engineering and Environmental Laboratory, P.O. Box 1625, MS 2218, Idaho Falls, ID 83415
Email: rnw2@inel.gov; Telephone (208) 526-6127; FAX (208) 526-4822

T.C. Totemeier
Idaho National Engineering and Environmental Laboratory, P.O. Box 1625, MS 2218, Idaho Falls, ID 83415
Email: totetc@inel.gov: Telephone (208) 526-3074; FAX (208) 526-4822

Manuscript

Corrosion-resistant coatings based on the iron aluminide intermetallic compound Fe_3Al are currently being investigated for fossil energy applications. Fe_3Al possesses excellent intrinsic high-temperature oxidation and sulfidation resistance, and a significant effort has been made in the development of bulk alloys based on it. While substantial progress has been made, the widespread use of these alloys has been hampered by a combination of low room-temperature ductility and high-temperature creep resistance [1]. The use of Fe_3Al as a coating material on a less corrosion-resistant substrate with more suitable mechanical properties offers one alternative for overcoming these limitations, with applications in the fossil energy industry.

The high-velocity oxy-fuel (HVOF) thermal spray process is a promising method of coating application. Fe_3Al coatings formed using this process are dense and well-bonded to the substrate. The residual stresses in the coating are typically compressive, due to the peening action of the lower-temperature, solid or semi-solid spray particles which impact the substrate at high velocity (~500 m/s). A recent study [2] has demonstrated that the magnitude of the residual stress can be controlled by varying the torch chamber pressure and hence the velocity of the spray particles.

Information on the mechanical and physical properties of Fe_3Al coatings is needed to enable more accurate modeling and prediction of coating behavior during formation and in service conditions. Data on actual coating material is required, since the coating properties are anticipated to be different than properties of bulk wrought material available in the literature. These differences arise from the complex coating microstructure and stress state. The coating microstructure features rapidly solidified splats, unmelted and partially melted spray particles, prior particle boundaries, oxide inclusions, small amounts of porosity, and high dislocation densities. Relatively high microhardness values for the coating in comparison with wrought Fe_3Al alloys were observed previously [2]; these were attributed to the complex microstructure.

The objective of the present study was to measure tensile strength and thermal expansion coefficients for HVOF Fe_3Al coatings produced with varied spray conditions. Coatings were prepared at three different torch chamber pressures, and were removed from the substrate prior to testing. The effect of annealing at 800°C for 2 hours on the tensile and expansion properties was assessed in an attempt to separate residual stress effects from microstructural effects. In addition to the property measurements, residual stresses in the as-sprayed coatings were characterized as a function of coating thickness using curvature measurements on coating-substrate couples.

Coating Preparation

Coatings were produced via HVOF thermal spraying in air at atmospheric pressure (85.5 kPa) using commercially available alloy FAS powder that has a nominal composition of Fe-28%Al-2Cr (atomic percent). AISI type 1020 low-carbon steel substrates were used, rectangular in shape with dimensions 76 x 12.5 mm. Coatings were sprayed on 1.4 mm thick substrates for residual stress measurements and onto 6.4 mm thick substrates for production of tensile specimens. Both sides of the substrates were grit blasted with Al_2O_3 particles prior to spraying so that the strips were nominally flat prior to coating.

The coatings were produced at an equivalence ratio of one (a stoichiometric mixture of kerosene and oxygen) and four torch chamber gage pressures: 170, 340, 517, and 620 kPa. Coatings with thicknesses ranging from 250 to 1500 μm were produced at each pressure for characterization of residual stresses as a function of thickness. Coatings with a minimum 1500 μm thickness were produced at three chamber pressures (170, 340, and 620 kPa) on the thicker substrates for microstructural examination, tensile testing, and coefficient of thermal expansion (CTE) measurements. The coatings were built up in layers by a raster deposition scheme. At a transverse velocity of 200 mm/s and a standoff distance of 355 mm, each pass of the substrate in front of the torch added an approximately 45 μm thick layer. Full details of the coating apparatus and parameters are given in Ref. [3].

Spray particle temperature and velocity characteristics were characterized for three chamber pressures (170, 340, and 620 kPa) using an integrated Doppler velocimeter and high speed two-color pyrometer [3, 4]. The estimated, one sigma, measurement uncertainties are 5% for particle temperature (assuming gray body behavior) and less than 5 m/s for particle velocity. Table I lists the relevant coating parameters, particle velocities, and temperatures. Consistent with previous investigations [2, 4, 5], the particle velocities increase with increasing chamber pressure, while particle temperatures are nearly constant for the constant equivalence ratio. Although it was not measured directly, the particle velocity for the 520 kPa chamber pressure was interpolated as 600 m/s for the purpose of residual stress comparison between the different conditions.

Table I. HVOF thermal spray particle characteristics

Chamber Pressure (kPa)	Equivalence Ratio	Particle Velocity (m/s)	Particle Temperature (°C)
170	1.0	390	1600
340	1.0	560	1650
620	1.0	620	1650

Microstructural Characterization

Residual stresses in the coatings were examined by measurement of the curvature of coating-substrate couples. As described above, the thickness of the coatings varied from 250 to 1500 μm while the substrate thickness was constant at 1.4 mm. Curvature measurement was performed using an optical comparator; stresses in the coating and substrate were calculated from curvature assuming linear elastic behavior and biaxial in-plane coating stresses. The full equations used for the calculation are developed in Refs. [6] and [7] and are summarized in Ref. [8]. Coating stresses were calculated at the surface, the coating-substrate interface, and the coating mid-plane. The stress at the coating mid-plane corresponds to an average coating stress for the linear behavior assumed.

Coating microstructures for three particle velocities (390, 560, and 620 m/s) were examined using standard metallographic techniques. The volume fractions of porosity and oxide phases were determined by image analysis of representative microstructures obtained using secondary and backscattered electron imaging. The fraction of apparent unmelted particles in the microstructures was determined by point count. The term “apparent” is used because the criterion for unmelted particles to be counted was a round or oval shape with clearly delineated border, and, at high spray particle velocities, some unmelted particles may have been so severely deformed by peening action that they did not meet this criterion. Hence the actual fraction of unmelted particles may be higher than indicated by optical assessment.

X-ray diffraction (XRD) was used to determine the degree of cold work present in the coatings through measurement of coherently diffracting domain size and microstrain (the Warren-Averbach method of line broadening analysis [9]). The profiles of the (110) and (220) peaks were measured for analysis and FAS powder was used as the strain-free standard. Measurements were made on a Bruker AXS D8 diffractometer using Cu K_a radiation produced at 40 kV and 30 mA.

Analysis was performed using the Bruker Crysize program following peak fitting with Pseudo-Voight functions. The equivalent dislocation density, ρ, for each condition was computed using the relationship [10]:

$$\rho = \frac{2\sqrt{3}\langle \varepsilon^2 \rangle^{1/2}}{|\vec{b}|\, D} \quad (1)$$

where the term $\langle \varepsilon^2 \rangle^{1/2}$ is the root mean square (RMS) microstrain, $\vec{b}$ is the Burger's vector, and D is the average column length. For the Fe_3Al coatings, the partial B2 dislocation Burger's vector was used (magnitude $\frac{\sqrt{3}}{2}a$,where a is lattice parameter).

Tensile Testing

Thin, dogbone shaped tensile specimens with a 25 mm gage length and 6.3 mm gage width were electro-discharge machined from the 1500 μm thick coatings. Because the coatings were not uniform in thickness (the center was considerably thicker than the edges), the final thickness of the specimens was 760 μm. The specimen had a pin-hole grip in order to minimize bending stresses, which were anticipated to be a problem with the brittle coatings. The specimens sprayed at higher velocities did have a slight curvature after separation from the substrate resulting from the residual coating stresses. Room temperature tensile tests were performed on as-sprayed and annealed coatings produced at three particle velocities (390, 560, and 620 m/s). Annealing of the specimens was performed at 800°C for 2 hours in air, with an air cool. 800°C lies in the disordered α phase field and has been previously shown to dramatically reduce the dislocation density in the coatings [2]. After failure in initial tests was observed to occur in the grip area, aluminum reinforcement tabs were expoxied onto the grip area. Holes were present in the tabs to allow for passage of the holding pins and to allow the pins to freely bear on the coating.

Two tests were performed at an elevated temperature of 700°C in air on coatings produced at a velocity of 560 m/s. A clamshell type resistance furnace was used for heating; the specimen temperature was measured using a type K thermocouple attached to the gage length. The use of a rod-in-tube type high-temperature extensometer on the thin coating specimens proved to be unsuccessful, and hence no modulus data is available for the high-temperature tests. The yield strength was estimated from load-crosshead displacement data. Post-test fractography was performed on selected specimens, by stereo light microscopic and scanning electron microscopic examination of fracture surfaces and metallographic cross-sections of fractured specimens. Cross-sections were prepared using standard metallographic techniques.

CTE Measurement

The mean CTE of the coatings was measured using a Theta Industries dilatometer operating in differential mode. Coating specimens 6.3 mm long were sectioned from the gage sections of tested tensile specimens; a Pt standard was used as the reference. The specimens were heated at 3°C/min in a rough vacuum; low contact forces were used to minimize creep deformation at high temperatures. Measurements were made on as-sprayed coatings produced at three particle velocities (390, 560, and 620 m/s); two specimens were tested for each velocity. Three sequential runs were performed on each specimen to observe changes in expansion behavior with thermal cycling.

Coating Microstructures

Data on the relevant microstructural features of coatings produced at particle velocities of 390, 560, and 620 m/s are listed in Table II. Coatings produced at the lowest velocity show considerable porosity, oxide, and a high apparent fraction of unmelted particles. Coatings produced at the higher velocities show essential zero porosity and a lower fraction of oxide. The apparent fraction of unmelted particles decreases with increasing particle velocity.

The X-ray line broadening analysis showed coatings sprayed at all velocities to be heavily cold-worked. Expressed in terms of equivalent dislocation density, the degree of cold work monotonically increases with increasing velocity, from 8.7×10^{10}

cm^{-2} at 390 m/s to $2.6x10^{11}$ cm^{-2} at 620 m/s. The dislocation density decreases following annealing at 800°C for two hours, although values are still significant. The amount of decrease is greater for higher-velocity coatings.

Table II. Coating microstructural features

Particle Velocity (m/s)	Apparent Fraction Unmelted Particles (vol%)	Fraction Porosity (vol%)	Fraction Oxide (vol%)
390	31	7	15
560	18	0	7
620	6	0	7

Residual Stress

The residual stress results obtained by curvature measurement are graphically depicted in Fig. 1. The stress levels in coatings sprayed at 390 and 560 m/s are essentially zero, and there is little variation with thickness. For the two higher velocities the residual stresses are compressive and increase with velocity. In thicker specimens sprayed at higher velocities, there is a substantial variation in stress across the coating thickness due to the large degree of bending, with tensile stresses at the coating surface and high compressive stresses at the coating-substrate interface. The average coating stresses (computed at the coating mid-plane) remain relatively constant with increasing coating thickness, however. For the coating sprayed at 600 m/s, the average coating stress is approximately −130 MPa, while for the 620 m/s coating the average coating stress is approximately −210 MPa.

Another measure of an "average" coating residual stress is the coating-substrate strain mismatch, $\Delta\varepsilon$, which is also calculated from curvature. This is the theoretical mismatch between the coating and substrate without allowing for energy minimization due to bending and can be considered the fundamental driving force for curvature development. Multiplication of $\Delta\varepsilon$ by the coating biaxial elastic modulus (201 GPa; the elastic modulus [11] divided by one minus Poisson's ratio) gives the stress that would theoretically have developed if the coating had been applied onto an infinitely thick substrate. The mismatch stresses for the 390 and 560 m/s coatings remain near zero, while for the 600 and 620 m/s coatings the mismatch stresses increase with coating thickness, in contrast to the average coating stresses (stress at coating midplane) for coatings sprayed onto thin substrates. The compressive mismatch stresses computed for the thickest coatings are quite high, −780 MPa for the 600 m/s coating and −1310 MPa for the 620 m/s coating.

Tensile Properties

The tensile test results at room temperature and 700°C are listed in Table III. The behavior of the coatings at room temperature was entirely brittle for all coatings, with failure in the elastic regime. As such, there was considerable scatter in the data, although trends are still readily discernable. The fracture stresses at room temperature increase with increasing particle velocity. In the as-sprayed condition, coatings produced at a velocity of 390 m/s failed at fairly low stresses (60-90 MPa). For a spray velocity of 560 m/s the range of fracture stresses increased to 190-240 MPa, while at 620 m/s the fracture stresses were 380 and 400 MPa. Interestingly, the elastic moduli also show large scatter and increase with spray particle velocity, from 70-100 GPa at 390 m/s to 120-150 GPa at 620 m/s.

Fracture stresses at room temperature increase considerably following annealing at 800°C. The magnitude of the increase is about a factor of three for the lowest velocity and nearly a factor of two for coatings sprayed at 560 m/s. Debonding of the aluminum reinforcement plates occurred for the two specimens sprayed at 620 m/s, therefore, the strengths reported (560 MPa) represent a minimum value since failure did not originate in the gage section. There were no significant differences in elastic modulus for the as-coated and annealed conditions. A small amount (approximately 1%) of ductility was observed in the two tests at 700°C. Both the yield strength and UTS were reduced at this temperature relative to the room temperature data.

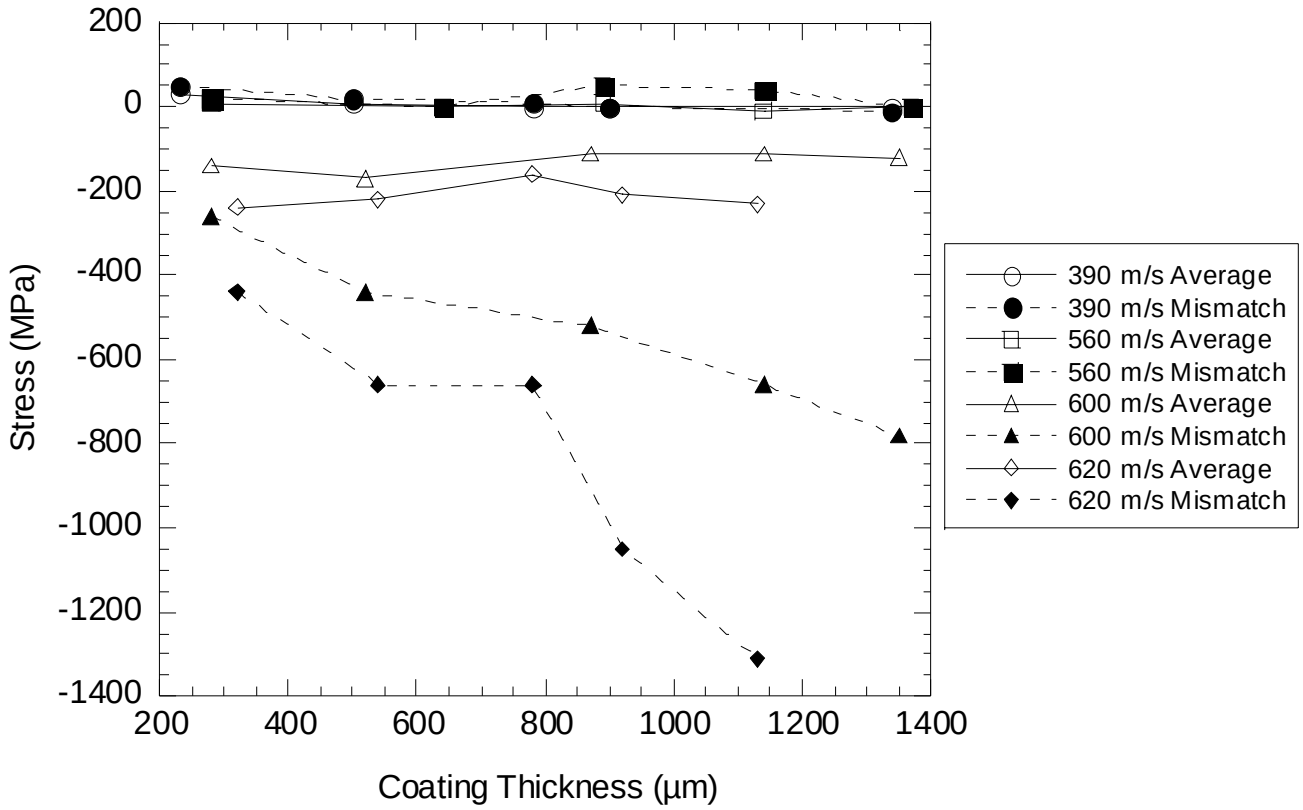

Figure 1. Coating residual stress as a function of coating thickness and particle velocity.

Similar failure features were observed for all conditions. Fracture was macroscopically brittle, oriented perpendicular to the applied stress. The fine-scale features were also brittle in nature, a mixture of separation along large, unmelted prior spray particles and fine-scale brittle fracture. The only discernable trend in fracture features is a qualitative decrease in the fraction of inter-particle separation with increasing spray particle velocity. There were no discernable differences in fracture features between as-coated and annealed coatings or between the coatings tested at room temperature and 700°C.

Thermal Expansion

Thermal expansion data for the coatings are presented in Fig. 2, which shows mean CTE as a function of temperature for coatings sprayed at velocities of 390, 560, and 620 m/s. Significant differences exist between the 1st and 3rd runs, and between the coatings and wrought Fe_3Al. The expansion of the coatings in the as-sprayed condition (1st run) was considerably less than that after two slow heating and cooling cycles to 1000°C (3rd run). Considerable scatter is seen in the coating data, particularly for the 1st run. Depsite the scatter, there are two significant features observed in the 1st run data—marked decreases in expansion at temperatures of 400 and 820°C. No significant trends in behavior as a function of spray particle velocity were observed.

All coating specimens showed a net shrinkage after cooling to room temperature following the first CTE run. The magnitude of shrinkage was relatively constant at approximately 0.5%; no trends with particle velocity were observed. The coating CTE data in the second and third runs (only third run shown) showed more consistent behavior in that similar trends in CTE with temperature were observed, although there was still scatter in magnitude. All plots show a marked cusp at approximately 550°C. Even in this annealed condition, the mean CTE values for the coatings are substantially lower than for wrought Fe_3Al. No dimensional changes were observed after the second and third CTE heating cycles.

Table III. Tensile Test Results

Test/Specimen ID	Particle Velocity (m/s)	Condition/ Test Temperature (°C)	Elastic Modulus (GPa)	Yield Stress (MPa)	UTS (MPa)	Elongation (%)
Fe3Al-25D	390	As-Coated, 25	--[a]	--	60	0
Fe3Al-25F	390	As-Coated, 25	--[a]	--	90	0
Fe3Al-25B	390	Annealed, 25	110	--	200	0
Fe3Al-25C	390	Annealed, 25	70	--	310	0
Fe3Al-50B	560	As-Coated, 25	110	--	190	0
Fe3Al-50C	560	As-Coated, 25	100	--	240	0
Fe3Al-50D	560	As-Coated, 25	80	--	200	0
Fe3Al-50F	560	As-Coated, 25	80	--	240	0
Fe3Al-50E	560	Annealed, 25	100	--	400	0
Fe3Al-50I	560	Annealed, 25	110	--	380	0
Fe3Al-50G	560	As-Coated, 700	--[b]	86	140	1
Fe3Al-50J	560	As-Coated, 700	--[b]	100	160	1.5
Fe3Al-90F	620	As-Coated, 25	140	--	400	0
Fe3Al-90B	620	As-Coated, 25	130	--	380	0
Fe3Al-90E	620	Annealed, 25	150	--	560	0
Fe3Al-90A	620	Annealed, 25	120	--	570	0

a: Failure loads too low for meaningful measurement.
b: Load-crosshead displacement data only.

Microstructure and Residual Stress

The observed dependence of microstructure, degree of cold work, and residual stress on particle velocity is consistent with conclusions of the initial study on HVOF Fe_3Al coatings [2]: Increasing velocity results in an increasing compressive peening contribution to residual stress. Increased peening also gives less porosity, fewer unmelted and undeformed particles, and a higher degree of cold work in the coatings, as evidenced by increasing dislocation density with increased particle velocity. As observed previously, annealing at 800°C reduces dislocation density through recovery and recrystallization.

While the general trends observed are consistent with the initial study, there are differences in magnitudes. In the initial study significant compressive residual coating stresses were observed at a 560 m/s particle velocity, while the stresses were essentially zero at this velocity in the current study. Also, significant porosity and oxides were observed at the 390 m/s particle velocity in this study, while essentially zero porosity, and low oxide levels, were observed previously. These differences are attributed to differences in the size distribution of the powders from which the coatings were sprayed; the powder in the previous study had a significant fraction of relatively large particles (approximately 50 μm diameter) which were not present in the powder used in this study. Due to their higher mass, larger particles impart a greater peening action at the same velocity, resulting in greater compressive stresses and reduced porosity. The peening effect has been previously shown to correlate with particle energy [5].

The variation in coating residual stress with increasing thickness, as characterized by coating-substrate curvature were additionally examined in this study. For the two velocities in which non-zero stresses were observed (600 and 620 m/s), the

amount of curvature increased with increasing coating thickness. The average coating stress (the stress calculated at the coating midplane) was relatively constant, however, and increased with increasing velocity, as expected due to increasing peening action.

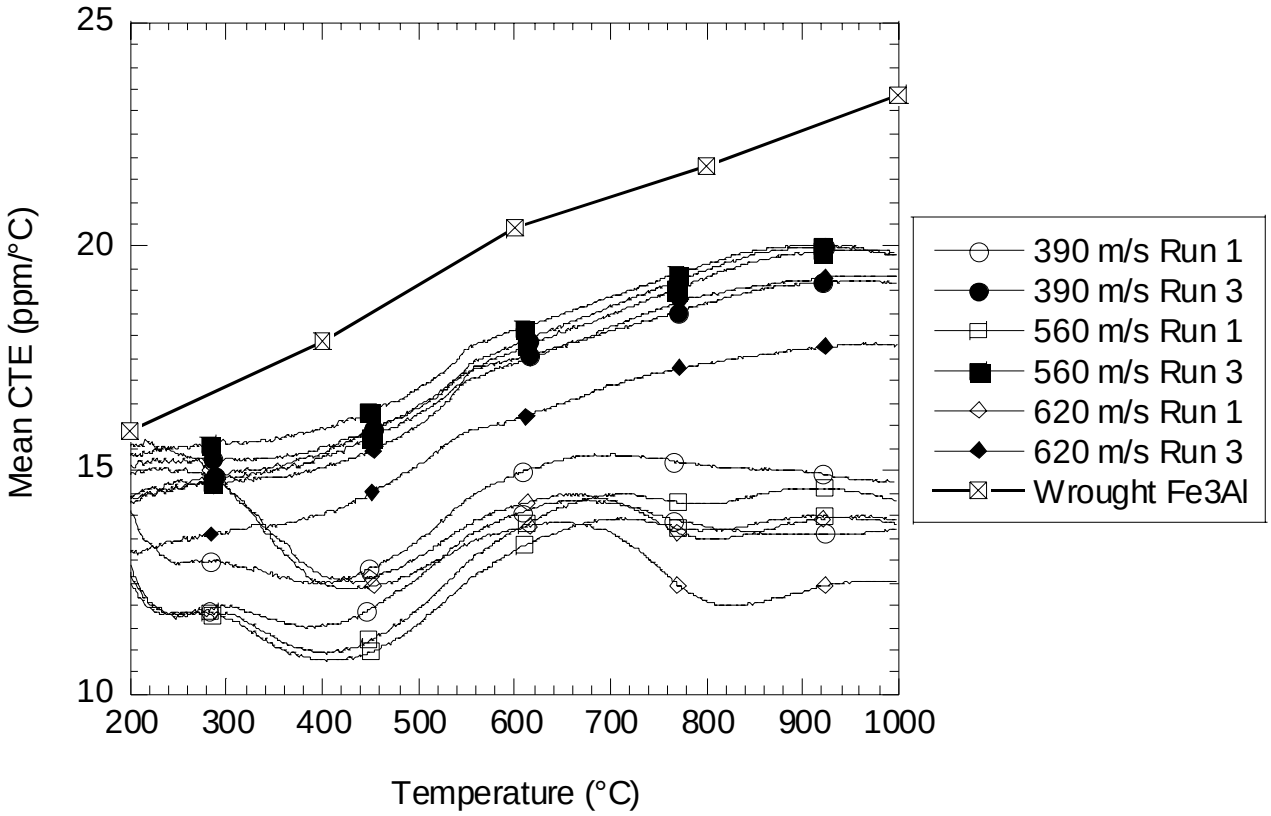

Figure 2. Mean CTE data for free-standing Fe_3Al coatings sprayed at different particle velocities. Data are presented for two specimens at each velocity and the first and third runs for each specimen. Data for wrought Fe_3Al are from Ref [11].

It is currently believed that the constant average stress may result from the application of the coating in discrete, ~40 μm thick layers. After each pass of the HVOF torch, the layer of coating applied equilibrates with the substrate to some degree, and the stresses resulting from coating deposition and cooling cause bending of the coating-substrate system. Hence the next layer of the coating is applied to an already curved substrate and a previously-deposited coating whose residual stresses are influenced by the bending which has occurred. This incremental action of deposition and bending is believed to result in an average coating stress that is independent of thickness. The average stress may therefore be a measure of the coating "deposition stress", i.e. the combination of the quench stress (resulting from solidification and rapid cooling of the coating splat), the peening stress, and the coating-substrate thermal mismatch stress (resulting from slower cooling of the coating-substrate couple between torch passes).

In contrast, the coating-substrate mismatch stresses monotonically increase with increasing coating thickness, to fairly high levels (nearly 1400 MPa) in the case of coatings prepared at 620 m/s. These stresses are calculated from curvature in an elastic, analytical model. The mismatch stress does not represent an actual stress in the curved coating-substrate couple, but rather the stress predicted to be developed if the coating were applied to a very thick substrate (no bending). The mismatch stress may therefore better represent the actual state of stress in service, where coatings are typically applied to thick substrates. The magnitude of these stresses are such that the coatings would likely crack or spall from the substrate at greater

thicknesses. Due to the incremental nature of coating application, however, these stresses may not develop in reality, since plastic deformation of the coating may occur as each layer cools between passes.

Residual stress development in HVOF-sprayed metallic coatings is being further studied using numerical modeling, comparison of residual stresses measured with X-ray analysis with those predicted from curvature measurements, and X-ray measurement of stresses in coatings applied to thick substrates. Numerical models which account for the complex nature of coating deposition have been previously developed [12], but have not as yet been applied to HVOF spraying of metallic materials, rather to plasma spraying. In the latter case, there is essentially no contribution of peening action to the residual stress due to low particle velocities.

Tensile Behavior

The tensile strength of HVOF-sprayed Fe_3Al coatings is dominated by brittle fracture behavior. No ductility was observed in any tests performed at room temperature, even after annealing of the coatings at 800°C. Such behavior is consistent with the limited room-temperature ductility observed for wrought iron aluminides [1]; the heavily cold-worked nature of the coatings and the significant fraction of brittle oxide inclusions also strongly promote brittle behavior. Increasing strength with particle velocity results from reduction in defects (in the form of porosity and oxides) and better bonding between spray particles. The latter factor is believed to account for the difference between coatings sprayed at 560 and 620 m/s, since they have identical porosity and oxide levels. Better inter-particle bonding with increasing velocity is apparent in the fracture paths .

It is more difficult to account for the consistent increase in strength with annealing at 800°C and the increasing modulus with increasing particle velocity. In former case, annealing may increase net fracture strength by removing local residual stresses within the coating (present even after removal from the substrate). The presence of residual coating stresses in the as-sprayed condition will reduce net strength by creating fracture-initiating high local stresses. Sufficient strengthening is apparently provided by the oxide inclusions, dislocations, and grain structure to raise the flow stress above the fracture stress even after annealing. This is supported by microhardness measurements presented in Ref. [2], in which hardness levels after one hour of annealing at 800°C corresponded to flow stresses ranging from 610 to 940 MPa, considerably greater than the fracture stresses measured in this study. There is currently no good explanation for the variation in elastic modulus, but it may stem from either coating residual stresses or the particular specimen geometry employed. The measured values of elastic modulus for the coatings sprayed at 620 m/s (120-150 GPa) do match those reported in the literature (145 GPa [11]).

The behavior of the two specimens tested at 700°C is consistent with that of wrought Fe_3Al alloys, in that the yield stress is considerably reduced above 600°C [13], and the ductility is increased. The coatings have considerably less ductility than typical wrought materials at this temperature, again likely resulting from weak inter-particle bonds and high oxide inclusion volume fraction.

Thermal Expansion

The results of the CTE measurements highlight the need for measurement of actual coating values rather than simply using those obtained on cast or wrought materials, since the coating CTE was significantly different from wrought material values, and the CTE significantly changed from the first to subsequent thermal cycles. The initial study [2] measured coating CTE values using XRD of coatings on substrates. The results of the present study, obtained using free-standing coatings and dilatometry, basically agree with the XRD results but are less ambiguous (due to lack of macroscopic residual stresses and substrate CTE effects) and provide better differentiation between the 1st and subsequent runs.

There is still considerable scatter between specimens, but significant differences are observed between the first run, on an as-sprayed coating, and subsequent runs in which the specimen is in an annealed state. The CTE values in the first run are significantly lower, and show two distinct regions of mean CTE decrease, at approximately 400 and 820°C. The magnitude of the difference in expansion between the first and subsequent runs correlates well with the net shrinkage of the specimen observed at room temperature after the 1st run. The differences in CTE are therefore attributed to microstructural changes which occur during heating of as-sprayed coatings to 1000°C.

Given the initial state of the coatings, there are a few processes by which net shrinkage of the coating could occur:

1. Reduction of vacancy and dislocation densities due to recovery and recrystallization;
2. Reduction in lattice parameter due to a higher degree of ordering;
3. Elimination of local residual stresses; and
4. Density increase due to sintering of porosity.

Of these, items 3 and 4 are not plausible in this case, since it is questionable that elimination of local residual stresses could give rise to the observed 0.5% change in length, and measurable porosity was only observed for coatings sprayed at 390 m/s. On the other hand, the transition from a disordered to B2 ordered structure gives rise to a 0.8% change in lattice parameter [14], and vacancy concentrations on the order of 0.2% and greater are not uncommon in quenched Fe-Al intermetallics [15]. Therefore, both ordering and recrystallization have the capacity to give rise to the observed shrinkage. Since the higher temperature decrease in mean CTE occurs at the recrystallization temperature for the FAS alloy [16], this clearly plays some role. Much of the remainder of the reduction in CTE appears to occur at fairly low temperature, suggesting that recovery processes or ordering may be operative.

After annealing, the variation in mean CTE with temperature is consistent. All runs show a distinct cusp at 550°C corresponding to the $D0_3$ to B2 transition temperature. Even in an annealed condition, however, the CTE values of the coating are lower than wrought values, by approximately 3 ppm/°C. The significant microstructural difference between an annealed coating and wrought material is the quantity of oxide present in the coating, which ranges from 7 to 15 vol% for the coatings considered. EDS analysis has shown this oxide to be principally alumina, which has mean CTE values that range from 6.5 to 8 ppm/°C for the temperature range considered [17]. Reduction of coating CTE values due to the presence of oxide inclusions is extremely plausible; simple rule-of-mixtures estimations of the net CTE for the mixture agree fairly well with the actual coating CTE. At 200°C, the calculated CTE is 14.7 ppm/°C, compared to 14.6 ppm/°C for the coating, and at 600°C the calculated CTE is 19.1 ppm/°C, compared to 17.8 ppm/°C for the coating.

Conclusions

1. As observed in previous work, peening stresses imparted by the high velocity spray particles induce compressive residual coating stresses and produce heavily cold-worked microstructures. The magnitude of peening effects increased with increasing particle velocity.

2. Net residual stresses in coatings sprayed at 390 and 560 m/s were near zero. For coatings sprayed at 600 and 620 m/s, the average residual stresses were nearly constant with increasing coating thickness, at −130 and −210 MPa, respectively. The coating-substrate mismatch strain, however, increased with increasing coating thickness.

3. The coatings exhibited brittle tensile behavior at room temperature. The fracture stress increased with increasing spray velocity, from 60-90 MPa at 390 m/s to 380-400 MPa at 620 m/s. Annealed coatings showed higher fracture strengths, which were hypothesized to be due to elimination of internal, local residual stresses.

4. The CTE values for the coatings were significantly lower than those of wrought Fe_3Al. As-sprayed coatings exhibit mean CTE values of approximately 12 ppm/°C; annealed coatings exhibit mean CTE values ranging from 15 to 20 ppm/°C. Differences between coatings and wrought materials are attributed to a 7-15 vol% fraction of oxide inclusions.

References

1. N.S. Stoloff: *Mater. Sci. Eng. A*, 1998, vol. A258, pp. 1-14.
2. T.C. Totemeier, R.N. Wright, and W.D. Swank: *J. Therm. Spray Technol.*, in press.
3. W.D. Swank, J.R. Fincke, D.C. Haggard, and G. Irons: in *Thermal Spray: Industrial Applications*, C.C. Berndt and S. Sampath, Editors, ASM International, Materials Park, OH, 1994, pp. 307-12.
4. W.D. Swank, J.R. Fincke, D.C. Haggard, G. Irons, and R. Bullock: in *Thermal Spray: Industrial Applications*, C.C. Berndt and S. Sampath, Editors, ASM International, Materials Park, OH, 1994, pp. 319-24.

5. S. Kuroda, Y. Tashiro, H. Yumoto, S. Taira, H. Fukanuma, and S. Tobe: *J. Therm. Spray Technol.*, 2001, vol. 10, pp. 367-74.
6. T.W. Clyne and S.C. Gill: *J. Therm. Spray Technol.*, 1996, vol. 5, pp. 401-18.
7. C.H. Hsueh and A.G. Evans: *J. Am. Ceram. Soc.*, 1985, vol. 68, pp. 241-48.
8. W.D. Swank, R.A. Gavalya, J.K. Wright, and R.N. Wright: in *Thermal Spray: Surface Engineering Via Applied Research*, C.C. Berndt, Editor, ASM International, Materials Park, OH, 2000, pp. 363-69.
9. B.E. Warren: *Prog. Metal Phys.*, 1959, vol. 8, pp. 147.
10. G.K. Williamson and R.E. Smallman: *Phil. Mag.*, 1956, vol. 1, pp. 34.
11. J.H. Schneibel: in *Processing, Properties, and Applications of Iron Aluminides*, J.H. Schneibel and M.A. Crimp, Editors, TMS, Warrendale, PA, 1994, pp. 329-42.
12. S.C. Gill and T.W. Clyne: *Metall. Trans. B*, 1990, vol. 21B, pp. 377-85.
13. C.G. McKamey, J.H. DeVan, P.F. Tortorelli, and V.K. Sikka: *J. Mater. Res.*, 1991, vol. 6, pp. 1779-805.
14. A.R. Yavari, D. Negri, E. Navarro, A. Deriu, A. Hernando, and W.J. Botta: *Journal of Metastable and Nanocrystalline Materials*, 1999, vol. 2-6, pp. 229-36.
15. I. Baker and P.R. Munroe: *International Materials Reviews*, 1997, vol. 42, pp. 181-205.
16. U. Prakash, R.A. Buckley, H. Jones, and C.M. Sellars: *ISIJ Int.*, 1991, vol. 31, pp. 1113-26.
17. W.D. Kingery, H.K. Bowen, and D.R. Uhlmann: *Introduction to Ceramics*, 2nd ed., Wiley Interscience, New York, 1976, pp. 593.